Pergamon

Int. J. Heat Mass Transfer. Vol. 40, No. 14, pp. 3419–3426, 1997

Printed in Great Britain
0017–9310/97 $17.00+0.00

PII: S0017–9310(96)00363–8

Ray effect in ray tracing method for radiative heat transfer

BEN-WEN LI and WEN-QUAN TAO
Division of Thermodynamics and Heat Transfer, School of Energy and Power Engineering, Xi'an Jiaotong University, Xi'an, Shaanxi 710049, People's Republic of China

and

RI-XIN LIU
R & D Center for Magnetic Materials, Beijing General Research Institute of Mining and Metallurgy, Fengtai, Beijing, 100054, People's Republic of China

(*Received* 20 *April* 1996 *and in final form* 20 *October* 1996)

Abstract—The ray effect in ray tracing method was analyzed and three new ray emitting methods for a surface element (method A, B and C) were presented. Numerical computations of viewfactors for three different typical configurations indicated that the proposed methods can significantly eliminate the ray effect. Compared with the conventional ray emitting method, the proposed methods, especially method C, can give much higher accuracy with less computer cost. In addition, the new method may have much wider range of applications. © 1997 Elsevier Science Ltd.

INTRODUCTION

Extensive researches have been done on the evaluation of diffuse view factors for irregular geometrical systems [1–3]. For planar surface systems the contour double integral formula (CDIF) can give results with higher accuracy even using simple formula [4]. The radiative heat transfer between such surfaces can be calculated easily. A comparative study of different numerical methods for evaluating the viewfactors of diffuse surfaces of arbitrary configuration was made by Emery *et al.* [5]. The Monte Carlo method is possibly the most flexible for the cases of irregular geometrical systems.

With the restraints of the RTE, a finite number of beams (bundles, particles, rays) are traced, and great pseudo-random numbers must be used for Monte Carlo method. The accuracy of the results mainly depends on the sample of beams and, hence, results fluctuate around the exact solution. Efforts are still needed to increase the accuracy as with the ray tracing method [6, 7], the uniform deterministic discrete method [8, 9] and the discrete techniques such as radiative heat ray method [10] and nonstochastic Monte Carlo [11]. The numerical computations for the determination of diffuse viewfactors of different cases indicated that the ray emitting method for ray tracing method cannot be applied to varied geometries for obtaining numerical solutions with high accuracy.

In the present study, the ray effect was analyzed and revised ray emitting methods were proposed. Numerical tests for three typical diffuse viewfactors indicated that these revisions can give much higher accuracy than that reported in Refs [6, 7].

ANALYSIS OF RAY EFFECT AND THE DESCRIPTION OF REVISED METHODS

Generally speaking, the procedure of the ray tracing method is nearly deterministic. For example, the emitting points on subelements are predetermined geometric uniformly and the directions of the beams are also predetermined with the condition that the radiative energy flux emitted by the subelement is equally distributed over the entire space around it. For a fixed number of beams, the group of directions which are measured by the longitude degree θ_i and the latitude φ_j, as shown in Fig. 4, are calculated just once for all, because every subelement has the same solid angle dividing of the entire space around it. Thus a great deal of pseudo-random numbers used in Monte Carlo can be avoided and due to the unbiased distribution of radiative energy flux around the entire space (for diffuse surface or isotropical radiative properties), there will not be any statistical errors or sampling bias.

Usually for a surface element the dividing of the whole 2π-steradian solid angle can be conducted on the hemispherical surface under the condition that all the solid angles are equal ($2\pi/N$ for a total N beams). Then, each beam is set in the direction of the ray which starts from the centre point of element and passes through the centroid of pencil. Let the radius of the hemisphere as unity, then any dividing method

NOMENCLATURE

A	transient variable for equation (4), curved surface element on hemisphere, area of surface zone [m^2]
$F_{i,j}$	viewfactor from surface i to surface j
ΔF	relative error of viewfactor
h_0	height of surface ③ in a channel in case 1
l_0	distance of the centres between the sphere and the surface element in case 3
N	total number of beams from one emitting point
N_p	number of emitting point
N_x, N_y	Number of emitting point in x and y coordinates, respectively
N_θ, N_φ	partition number in θ and φ in directions
r	radial direction coordinate [m]
R	radius of sphere, value of unity
V	volume of pencil [m^3]
x, y, z	Cartesian coordinate location [m]
$\bar{x}$, $\bar{y}$, $\bar{z}$	Cartesian coordinate location of centroid [m]
z_0	height of the cylinder in case 2.

Greek symbols

θ	circumferential angle [rad]
φ	polar angle measured from normal vector of a surface [rad]
Ω	domain of integration.

Subscripts

a	analytical.

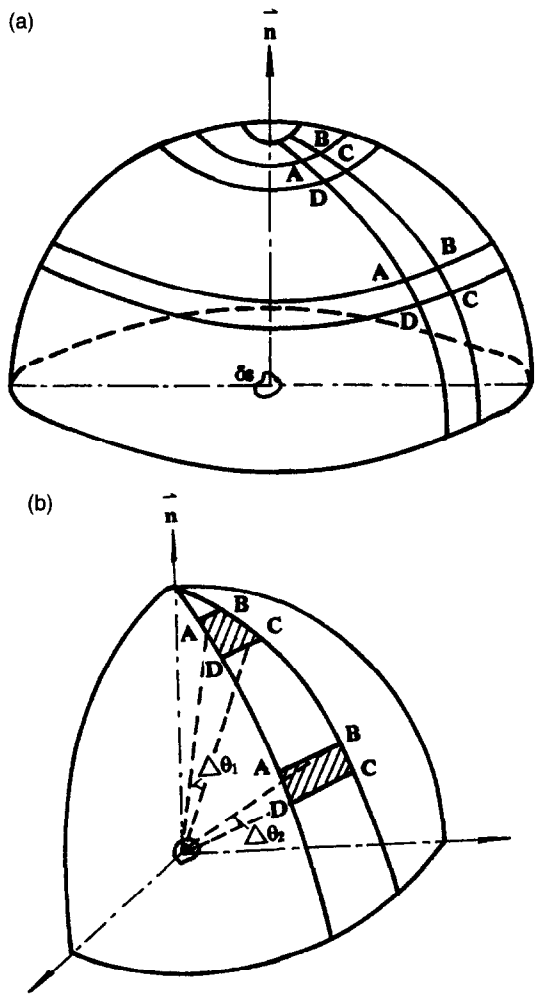

Fig. 1. (a) Spherical surface dividing method A; (b) ray effect in spherical surface dividing.

which can make each curved element equal to $2\pi/N$ is acceptable. However, from the authors' practice it is interesting to note here that the proper dividing of element in the hemisphere, i.e. the proper description of solid angles in space, is of great importance to the numerical solution. In the following three revised ray emitting methods (i.e. three element dividing methods) will be proposed. In the subsequent section, they will be used to determine the viewfactors of three diffuse configurations and some comparison will be made.

Let the elemental longitude angle be $2\pi/N_\theta$ and the number of the elemental latitude angle be N_φ, then, for a hemisphere space the total number of beams is $N_\theta * N_\varphi$, each of which is confined in an elemental solid angle of $2\pi/(N_\theta * N_\varphi)$. However, if there is a spherical crown element at the top of the sphere (Fig. 1(a)), the total number of beams will be $N_\theta * N_\varphi + 1$ and this dividing method is called method A, in which the elemental solid angles of each beam are equal.

Let us pay attention to an arbitrary curved element ABCD on a hemisphere surface shown in Fig. 1(b). For the same element longitude angle, the shape of the element depends on its position. If ABCD is closed to the top of the hemisphere, the arc length of (AD + BC) is greater than that of (AB + CD). While if ABCD is closed to the bottom, the situation is just opposite. In other words, even for the equal elemental solid angle $2\pi/N$, the shape of the curved quadrilaterals on the hemisphere surface can be very different. This phenomenon may significantly affect the accuracy of numerical solution by ray tracing method, just like the "ray effect" in discrete ordinates method. Numerical examples will be provided in the following section.

Now another two dividing methods will be introduced. Attention will be focused on the octant of a

hemisphere. First, the whole hemisphere surface is divided into many spherical rings. Then from the top to the bottom, each ring is divided into different number of elements and the element numbers in the successive spherical rings constitute an arithmetic progression. There are several choices for the number of elements of the top zone (say 1, 2 and 3) and the value of the common difference (say 1, 2 or 3). From our numerical practice, among the many combinations of the element number of the top zone and the common difference, there are two ways which can give good accuracy with the same common difference 1. In one way the first spherical zone on the top of the sphere reduces to a crown (Fig. 2, method B). In the second way, the first spherical zone reduces to two elements (Fig. 3, method C). The same dividing procedure can be conducted for the other three octants of the hemisphere.

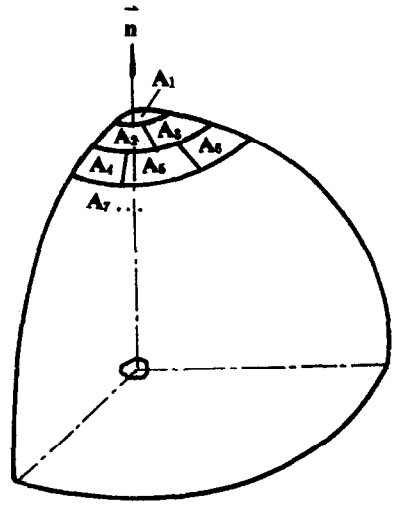

Fig. 2. Spherical surface dividing method B.

The determination of ray's direction (θ_i, φ_j) is a geometrical problem. For any curved surface element (ABCD in Fig. 4), the angles $\theta_1, \theta_2, \varphi_1, \varphi_2$ can be easily calculated. Then the location of the centroid $G(\bar{x}, \bar{y}, \bar{z})$ can be calculated through a series of integration within the domain $\Omega: 0 \leqslant r \leqslant R, \theta_1 \leqslant \theta_i \leqslant \theta_2, \varphi_1 \leqslant \varphi_j \leqslant \varphi_2$

$$\begin{cases} \bar{x} = \dfrac{1}{V}\iiint_{\Omega} x \, dV \\ \bar{y} = \dfrac{1}{V}\iiint_{\Omega} y \, dV. \\ \bar{z} = \dfrac{1}{V}\iiint_{\Omega} z \, dV \end{cases} \tag{1}$$

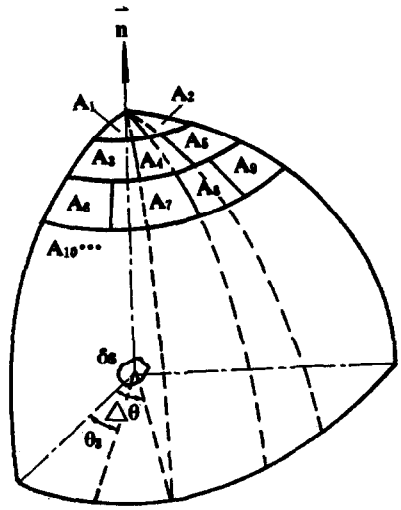

Fig. 3. Spherical surface dividing method C.

Equation (1) can be integrated through the transform from spheroidal into Cartesian coordinates. First:

$$V = \int_{\theta_1}^{\theta_2} d\theta \int_{\varphi_1}^{\varphi_2} \sin\varphi \, d\varphi \int_0^R r^2 \, dr$$

$$= (\theta_2 - \theta_1)(\cos\varphi_1 - \cos\varphi_2)\frac{R^2}{3}.$$

Similarly

The ray $\overrightarrow{OG}$ is the beam direction in solid angle O–ABCD (Fig. 4). So

$$\varphi_j = tg^{-1}\left(\frac{\sqrt{(\bar{x})^2 + (\bar{y})^2}}{\bar{z}}\right) \tag{3}$$

Set

$$\begin{cases} \bar{x} = \dfrac{3R(\sin\theta_2 - \sin\theta_1)[2(\varphi_2 - \varphi_1) - (\sin 2\varphi_2 - \sin 2\varphi_1)]}{16(\theta_2 - \theta_1)(\cos\varphi_1 - \cos\varphi_2)} \\ \bar{y} = \dfrac{3R(\cos\theta_1 - \cos\theta_2)[2(\varphi_2 - \varphi_1) - (\sin 2\varphi_2 - \sin 2\varphi_1)]}{16(\theta_2 - \theta_1)(\cos\varphi_1 - \cos\varphi_2)} \\ \bar{z} = \dfrac{3}{8}R(\cos\varphi_1 + \cos\varphi_2). \end{cases} \tag{2}$$

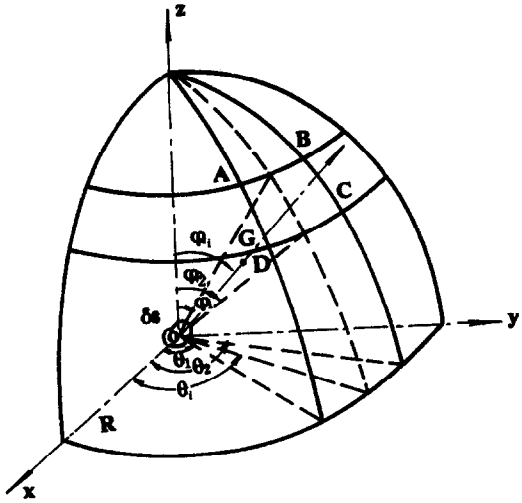

Fig. 4. Illustration of the calculation of ray's direction.

$$A = \frac{3R[2(\varphi_2-\varphi_1)-(\sin 2\varphi_2-\sin 2\varphi_1)]}{16(\theta_2-\theta_1)(\cos\varphi_1-\cos\varphi_2)}.$$

Equation (3) can be rewritten as

$$\varphi_j = tg^{-1}\left\{\frac{A\sqrt{2[1-\cos(\theta_2-\theta_1)]}}{(3/8)R(\cos\varphi_1+\cos\varphi_2)}\right\}. \quad (4)$$

The longitude angle θ_i can be calculated easily. For example, as to the second spherical ring in Fig. 3 (elements A_3, A_4, A_5 are shown there), the $\Delta\theta$ is $(\pi/2)/3$ and

$$\theta_3 = \tfrac{1}{2}\Delta\theta. \quad (5)$$

NUMERICAL TEST AND COMPARISONS WITH THE PREVIOUS RESULTS REPORTED

For the initial direction (θ_i, φ_j), the same formula used in both Refs [6, 7] will be adopted. In terms of the symbols used in the present paper, it can be written as:

$$\begin{cases} \theta_1 = \varphi_1 = 0 \\ \theta_i = 2\pi(i-1)/N_\theta, i \neq 1 \\ \varphi_j = \left\{\begin{matrix}\sin^{-1}[(1+jN_\theta-N_\theta)/(N_\theta N_\varphi+1)]^{0.5} \\ +\sin^{-1}[(1+jN_\theta)/(N_\theta N_\varphi+1)]^{0.5}\end{matrix}\right\}/2, \quad j \neq 1. \end{cases} \quad (6)$$

However, it should be noted that for the different cases used in Refs [6, 7], the effect of the ratio N_θ/N_φ on the numerical accuracy when keeping the total number $(N_\theta \times N_\varphi + 1)$ constant seems very different. As described in Ref. [6], for its calculated case (Fig. 3 in Ref. [6]) the relative error ΔF keeps small for the range of $4 \leqslant N_\theta/N_\varphi \leqslant 16$ and the values of $N_\theta = 80$, $N_\varphi = 20$ $(N_\theta/N_\varphi = 4)$ were used finally. While in Ref. [7], for its calculated case (Fig. 3 in Ref. [7]), the authors claimed that: "sufficient accuracy is obtained for $N_\theta = N_\varphi \geqslant 40$" and the values of $N_\theta = N_\varphi = 40$ $(N_\theta/N_\varphi = 1)$ were used finally. Therefore, it can be concluded that, the appropriate range of the ratio N_θ/N_φ is highly problem-dependent when N_θ and N_φ were calculated by the equation (6).

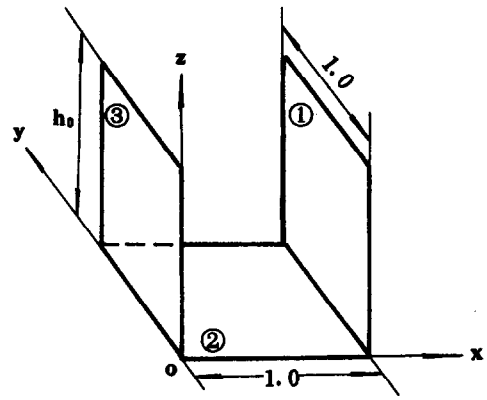

Fig. 5. Radiation model of a channel with rectangular surfaces.

In order to check the revised ray emitting methods, three different cases will be adopted in which the viewfactors for three diffusive configurations are calculated. For comparison purpose, the numerical error ΔF is defined in the same way as that in Refs [6, 7], with its subscript 1, 2, 3, 4 standing for the results from Refs [6, 7] and method A B and C of this paper, respectively.

Case 1

As adopted from Ref. [6], a channel shown in Fig. 5 is considered here. The channel is composed of three rectangles ①, ② and ③. Let the value of h_0 be 1.0, 2.0 and 5.0, the viewfactors of surface ② to surface ①, $F_{2,1}$, were computed using formula (6) and method A, B and C, respectively. The exact viewfactors, $F_{2,1}$ or $F_{2,3}$, can be calculated by means of the contour-integral method using Stokes' theorem. For $\Delta F_1 \sim \Delta F_4$, keep the number of rays from one emitting element constant, 101 $(N_\theta \times N_\varphi = 20 \times 5, N_\theta/N_\varphi = 4)$ for ΔF_1, 101 $(N_\theta \times N_\varphi = 10 \times 10)$ for ΔF_2, 60 $(4 \times (1+2+,\cdots,+5))$ for ΔF_2 and 56 $(4 \times (2+3+4+5))$ for ΔF_4, then increase the emitting points N_p ($N_p = N_x \times N_y$ in x and y coordinates respectively and $N_x = N_y$), the ΔF are computed accordingly for different values of h_0. The results are shown in Figs. 6–8.

It is very clear from Fig. 6 that, with the increasing

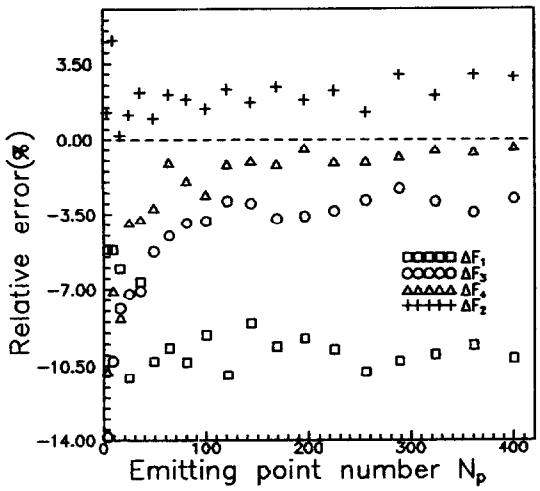

Fig. 6. Relative errors with the increasing of emitting point number N_p ($h_0 = 1.0$).

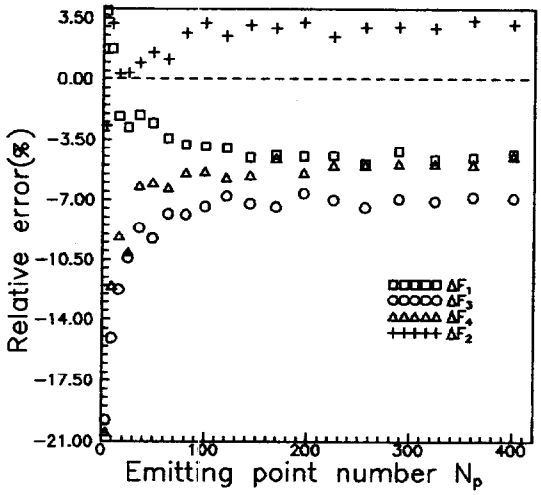

Fig. 7. Relative errors with the increasing of emitting point number N_p ($h_0 = 2.0$).

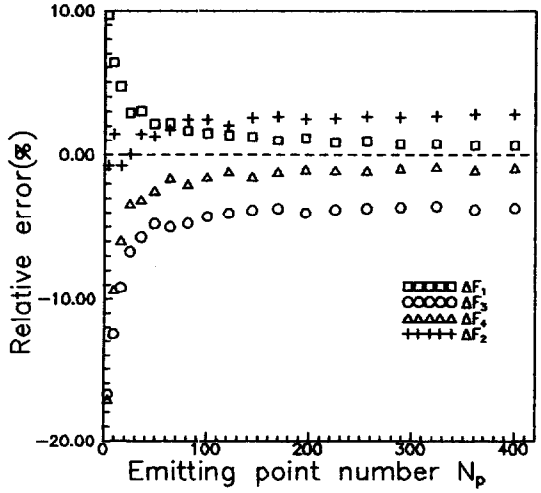

Fig. 8. Relative errors with the increasing of emitting point number N_p ($h_0 = 5.0$).

of N_p, the absolute value of the relative errors of ΔF_3, ΔF_2 quickly decrease to less than 3.5%, especially that of ΔF_4 decreases to less than 1%, but that of ΔF_1 remains as high as greater than 8%. Figures 7 and 8 show that the absolute values of ΔF_1 and ΔF_4 almost have the same value when the emitting point N_p is greater than 100. Finally, it can be seen that for different values of h_0, ΔF_1–ΔF_4 keep almost unchanged when N_p is greater than 100 ($N_x \times N_y = 10 \times 10$). Generally speaking, the accuracy of the viewfactors will be improved gradually with increasing N_θ and N_φ when the emitting point N_p keeps constant. For example, for sufficient accuracy of viewfactors of finite element to surface, the number of rays should be as high as $N_\theta \times N_\varphi = 1600$ [6, 7]. Keep the emitting point N_p constant and increase the ray number from one point, the comparison of accuracy for the above methods can be found in Ref. [9].

Case 2

This case is copied from Ref. [7] (see Fig. 9). The radius of the disk is taken as unity. $F_{d2,1}$ is computed for different height of the cylinder, $z_0 = 0.2$, 0.5, 0.9 and 1.5. The analytical solution of $(F_{d2,1})_a$ is presented in Ref. [12]. Due to the practice of Ref. [7], the ratio of N_θ/N_φ in equation (6) should always be 1 for different number of ray. The same ratio was used for method A, and the results are shown in Figs. 10–13 for different z_0.

From the results methods B and C have almost the same convergence speed and for different z_0 their relative errors ΔF decrease to less than 2% when the number of rays is greater than 300. However, the results of equation (6) seem to be irregular for different z_0 and the average absolute values of the relative error increase with the increasing of z_0. As for the method A, its numerical errors are greater than those of method B and C, but less than that of equation (6) and in some case, for example $z_0 = 0.2$, approach that of method C.

According to Ref. [7], good accuracy may be obtained if the number of rays is big enough ($N_\theta = N_\varphi \geqslant 40$). For the purpose of testing, the great enough numbers of rays (even as high as 10 000) were

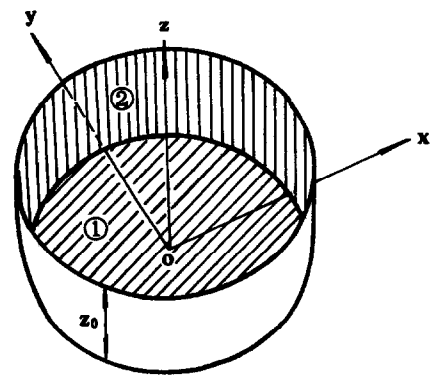

Fig. 9. Radiation model of a configuration consisting of a disk and a cylinder.

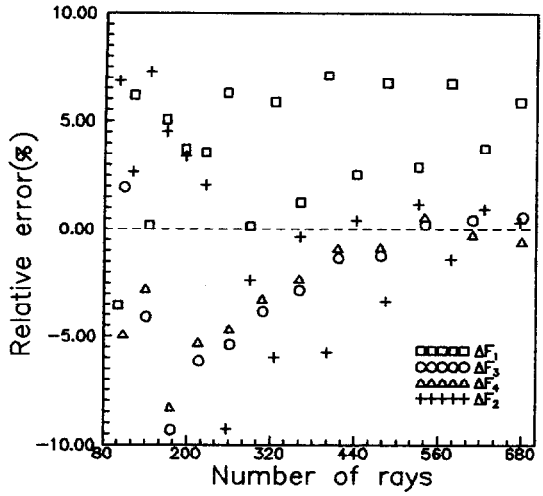

Fig. 10. Relative errors with the increasing of rays ($z_0 = 0.2$).

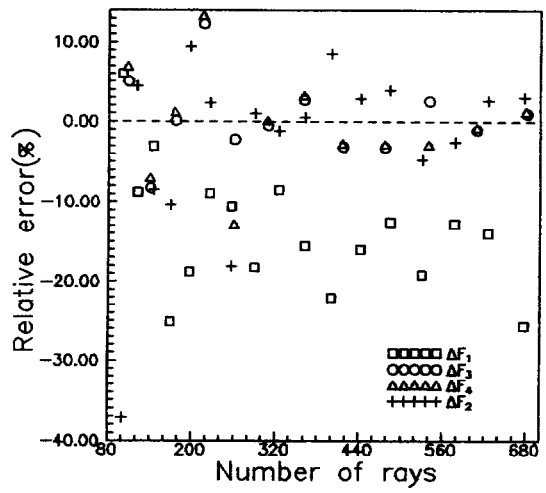

Fig. 13. Relative errors with the increasing of rays ($z_0 = 1.5$).

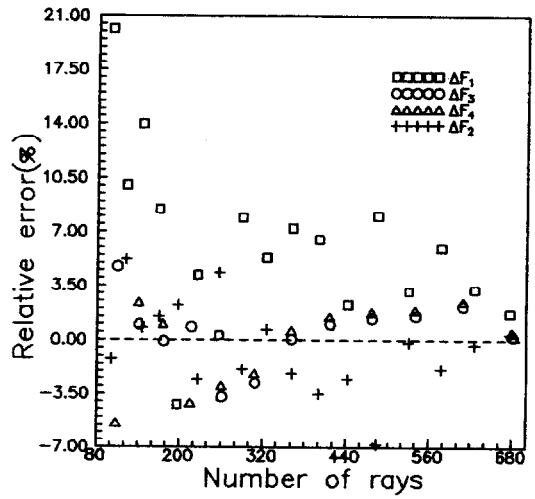

Fig. 11. Relative errors with the increasing of rays ($z_0 = 0.5$).

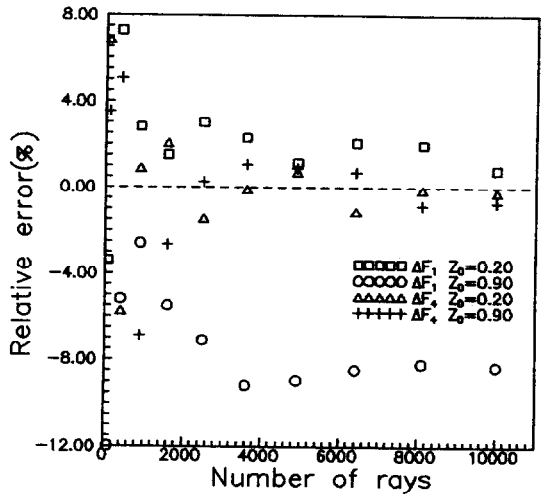

Fig. 14. Relative errors with the increasing of rays.

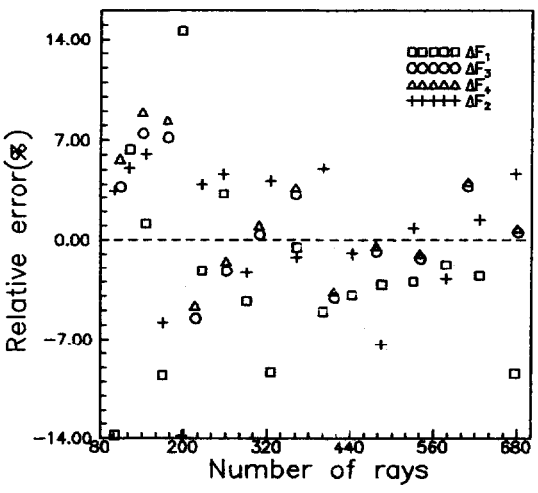

Fig. 12. Relative errors with the increasing of rays ($z_0 = 0.9$).

used for the cases of $z_0 = 0.2$ and 0.9 with equation (6) and method C, respectively. It can be seen from the results (Fig. 14) that the relative errors of equation (6) decreases very slowly when the number of rays is greater than 2000 and keeps a relatively high level finally. However, that of method C is just opposite with an error less than 1.5% when the number of rays is greater than 2000.

Case 3

In order to examine the flexibility of the revised methods, another configuration which consists of a surface element and a sphere (Fig. 15) was considered. The radius of sphere is taken as unity, the viewfactors of dA_1 to the sphere were computed using equation (6) and method A, B and C under the conditions of $l_0 = 1.2$, 1.5 and 1.9. The analytical values of $F_{d_1,2}$ was obtained by the formula in Ref. [13]. For equation (6) and method A, the values of $N_\theta = N_\varphi$ was used for different number of rays.

From the results (Figs. 16–18), method B and C

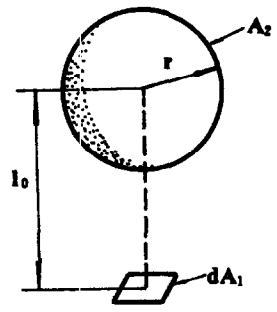

Fig. 15. Radiation model of a configuration consist of a surface element and a sphere.

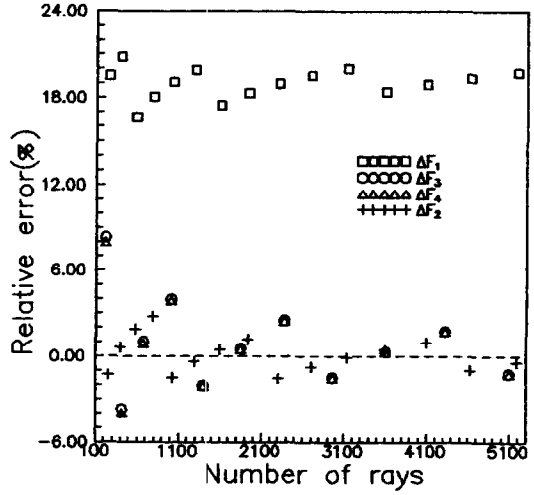

Fig. 16. Relative errors with the increasing of rays ($l_0 = 1.2$).

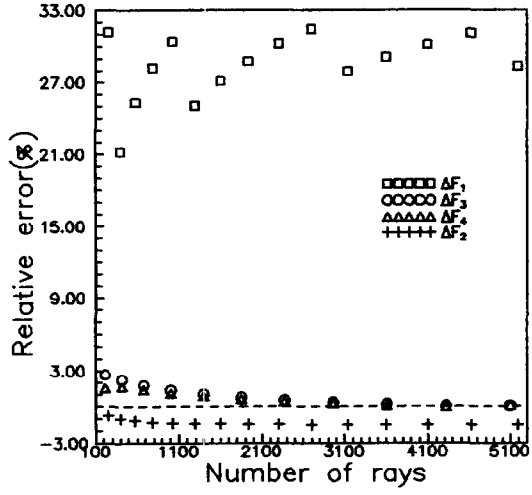

Fig. 17. Relative errors with the increasing of rays ($l_0 = 1.5$).

have almost the same relative errors for different l_0, and their accuracies are high enough to be accepted when the number of rays was greater than 1200. The same conclusion may be obtained for method A except for its little higher relative error than those of method B and C. Unfortunately, the relative errors of equation (6) always kept very high for different l_0 which even

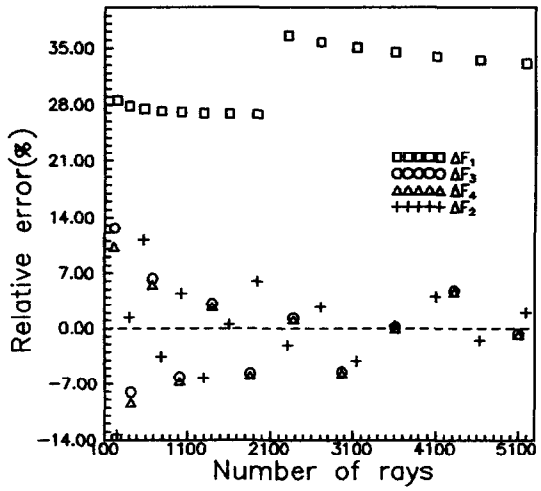

Fig. 18. Relative errors with the increasing of rays ($l_0 = 1.9$).

could not be less than 10% finally with the increasing number of rays. Similar results were obtained for the range of $4 \leqslant N_\theta/N_\varphi \leqslant 16$ when using equation (6).

CONCLUSIONS

The ray effect in conventional ray tracing method was analyzed and three revised ray emitting methods for a surface element were proposed which can significantly discard the ray effect. The numerical computation of the diffuse viewfactors for three different geometrical systems by the three new methods show good agreement with analytical solutions, and much higher accuracy can be obtained with the revised methods proposed as compared with the conventional one. According to the numerical test, the revised method C would be the best one for discarding ray effect and the flexibility of the ray tracing method can be greatly improved. The revised methods proposed can be used to evaluate the radiative heat transfer directly for arbitrary bodies with specular and/or diffuse surfaces [6, 7], or to determine the radiative direct exchange areas of irregular geometric systems [9].

Acknowledgements—This work was financially supported by the National Postdoctorial Research Fund, China.

REFERENCES

1. Eddy, T. L. and Nielesson, G. E., Shape factors for channels with varying cross-sections. *ASME Journal of Heat Transfer*, 1988, **110**, 264–266.
2. Chung, T. J. and Kim, J. Y., Radiative viewfactors by finite elements. *ASME Journal of Heat Transfer*, 1982, **104**, 792–795.
3. Brockmann, H., Analytic angle factors for the radiant interchange among the surface elements of two concentric cylinders. *International Journal of Heat and Mass Transfer*, 1994, **37**(7), 1095–1100.
4. Ambirajan, Amrit and Venkateshan, S. P., Accurate determination of diffuse viewfactors between planar surfaces. *International Journal of Heat and Mass Transfer*, 1993, **36**(8), 2203–2208.

5. Emery, A. F., Johansson, O., Lobo, M. and Abrous, A., A comparative study of methods for computing the diffuse radiation viewfactors for complex structures. *ASME Journal of Heat Transfer*, 1991, **113,** 413–422.
6. Maruyama, S., Radiation heat transfer between arbitrary three-dimensional bodies with specular and diffuse surfaces. *Numerical Heat Transfer*, Part A, 1993, **24,** 181–196.
7. Maruyama, S. and Aihara, T., Radiation heat transfer of a Czochralski crystal growth furnace with arbitrary specular and diffuse surfaces. *International Journal of Heat and Mass Transfer*, 1994, **37**(12), 1723–1731.
8. Ben-Wen Li, Hai-Geng Chen and Bao-Lin Ning, Uniform deterministic discrete method for radiative viewfactors in complex geometric systems. *Journal of Thermal Science*, 1995, **4**(2), 100–103.
9. Ben-Wen Li and Wen-Quan Tao, Uniform deterministic discrete method for radiative heat transfer in three-dimensional systems. *Chinese Journal of Chemical Engineering* (submitted).
10. Katayama, T., Radiative heat transfer analysis by the radiative heat ray method. *Transactions of JSME*, 1986, **52,** 1734–1740.
11. Murty, C. V. S., Evaluation of radiation reception factors in a rotary kiln using a modified Monte Carlo scheme. *International Journal of Heat and Mass Transfer*, 1993, **36**(1), 119–132.
12. Howell, J. R., *A Catalog of Radiation Configuration Factors*. McGraw-Hill, New York, 1982.
13. Siegel, R. and Howell, J. R., *Thermal Radiative Heat Transfer*. Hemisphere, New York, 1981.